Preparation of Poly(methyl methacrylate) Nanocomposites with Superior Impact Strength

Dhananjay Singh,[1,2] T. Jayasimha,[1] K. N. Rai,[1,2] Anil Kumar[1]

[1]*Department of Chemical Engineering, Indian Institute of Technology, Kanpur, India 208016*
[2]*Material Science Program, Indian Institute of Technology, Kanpur, India 208016*

Received 25 September 2006; accepted 13 February 2007
DOI 10.1002/app.26478
Published online 17 May 2007 in Wiley InterScience (www.interscience.wiley.com).

ABSTRACT: A chemically stable syrup of poly(methyl methacrylate) in its monomer was prepared with a suitable dual-initiating system. Nanoalumina particles were prepared by the autoignition of aluminum nitrate with urea and were made compatible with the organic medium by chemical modification with methacrylol isocyanate. The polymer syrup prepared in this way was applied between two poly(methyl methacrylate) sheets (each 10 cm × 10 cm × 2 mm), and the composite thus prepared was tested with a bullet-firing machine and a drop-weight-impact testing machine. The impact strength measurements of the two-plate composite from both of these procedures showed that the impact resistance doubled in the case of nanoalumina. The modeling of the damage to the multilayered composite by the critical impact energy was performed with the relation $E = pn^2 + qn + r$, where E is the impact energy, p, q, and r are constants, and n is the number of layers. Experiments showed that the presence of nanoparticles in the adhesive increased the value of the constants. The 10-layer composite was further tested with a 0.32 Indian Ordinance Factory (IOF) revolver with a bullet mass of 9.9 g and a muzzle velocity of 236 ± 7 m/s (muzzle energy = 275 J) from a 10-m distance, which produced an ordinary indentation with no penetration. © 2007 Wiley Periodicals, Inc. J Appl Polym Sci 105: 3183–3194, 2007

Key words: adhesion; composites; impact resistance; nanotechnology; strength

INTRODUCTION

Polymer nanocomposites[1] have attracted attention recently because of their superior mechanical properties over their constituents due to synergistic interactions between the dispersed particulates and polymer matrices.[2,3] Traditionally, people have employed micrometer-size inorganic particulates in polymer matrices in an attempt to improve the mechanical properties. However, the filler contents needed for such improvements are as high as 20 vol%,[4,5] and this high filler content causes deterioration in the processing of the polymer. Because of this, attempts have been made to synthesize a composite with much lower particle (in the range of nanodimensions) concentrations involving filler fractions in the range of 1–2%.[6] This technique brings significant improvements in the brittle fracture[7–9] and toughness[10,11] of nanocomposites. Ash et al.[12] briefly reported the tensile behavior of spherical nanoparticle alumina-filled poly(methyl methacrylate) (PMMA), and the most significant result was the increase in the strain to failure, which averaged over 28% in 5 wt % filled samples. The process of synthesizing polymer nanocomposites has been reported to involve three basic processes: (1) the synthesis of inorganic/ceramic nanoparticles, (2) the synthesis of a suitable polymer, and (3) the uniform dispersion of the nanoparticles in the polymer matrix. These three processes can be used sequentially or monolithically, depending on the specific need.

There are several types of nanoparticles such as inorganic oxides (e.g., alumina and silica) and metal particles (e.g., silver and copper) that can be synthesized by techniques such as coprecipitation, sol–gel processing, microemulsion, hydrothermal/solvothermal,[13] and autoignition techniques. In the coprecipitation technique,[14,15] the nanoparticles are formed through steps such as chemical reactions, nucleation, growth, coarsening, and/or agglomeration.[16–18] Sol–gel processing refers to the hydrolysis and condensation of alkoxide-based precursors such as tetraethyl orthosilicate[19] and consists of steps such as the formation of a sol and then its reaction to produce an oxide- or alcohol-bridged network (the gel).[20–22] This is followed by the aging and drying of the gel and the subsequent densification and decomposition of the gels at high temperatures (≥800°C). Liu et al.[23] in this way prepared nano-Ti-doped SnO_2 powder, and Wang et al.[24] prepared nanoaluminum borate wires.

Hydrothermal/solvothermal processing consists of carrying out a chemical reaction at a high tempera-

K. N. Rai is an Emeritus Fellows of All India Council of Technical Education.

Correspondence to: A. Kumar (anilk@iitk.ac.in).

ture and pressure, and when the medium is water, it is called hydrothermal processing.[25–27] Yang et al.[28] used this technique for the preparation of nanoparticles of transition-metal diselenides (MSe_2, where M is Ni, Co, or Fe). In the microemulsion technique, two reactants (A and B) are reacted in microemulsions.[29–33] Agostiano et al.[34] used this technique for the preparation of CdS nanoparticles from water-in-oil microemulsions. Autoignition processing is a simple method for the preparation of nanoalumina powders. In this method, through a heat treatment around 500–600°C only, nanocrystalline α-alumina powders have been obtained.

There are several processing techniques for preparing polymer matrix nanocomposites, and two of these are melt mixing and *in situ* polymerization. Vollenberg and Heikens[35] were able to produce good nanocomposite samples by thoroughly mixing filler particles with polymer matrices. The polymer matrices used in these experiments were polystyrene, a styrene–acrylonitrile copolymer, polycarbonate, and polypropylene. The inclusions were alumina beads 35 and 400 nm in size and glass beads 4, 30, or 100 μm in diameter. Chan et al.[36] made nanocomposites with a polypropylene matrix and calcium carbonate ($CaCO_3$) through the melt mixing of the components. Polyurethane–silica nanocomposites were made by Petrovic et al.[37] through the mixing of the silica with the polyol.

In situ polymerization is a technique that has been used to make polymer matrix nanocomposites.[38–40] In this method, first nanoparticles are dispersed in the monomer, and then the mixture is polymerized. Nanocomposites with a polyamide-6 matrix and silica inclusions were produced through the drying of the particles to remove any water absorbed onto the surface. Then, the particles were mixed with ε-capromide, and concurrently, a suitable polymerization initiator was added. The mixture was then polymerized at a high temperature under nitrogen. Li et al.[41] used a different approach to prepare high-density polyethylene (HDPE)/polypropylene nanocomposites. About 75 wt % HDPE and 25 wt % polypropylene were melt-mixed and extruded into tapes. This produced a nanocomposite with HDPE as the matrix and polypropylene fibrils ranging from 30 to 150 nm in diameter. For clay nanocomposites, the specific choice of the processing steps depends on the final morphology required in the composite, that is, an exfoliated or intercalated form.[42,43]

Qi et al.[44] prepared acrylate polymer/silica nanocomposite particles through miniemulsion polymerization by using a methyl methacrylate (MMA)/butyl acrylate mixture containing well-dispersed nanosized silica particles coupling-treated with 3-(trimethoxysilyl)propyl methacrylate. Mori and Saito[45] proposed a novel synthetic method for PMMA/silica nanocomposites with well-segregated PMMA and silica domains. To obtain the nanocomposite, a poly(methyl methacrylate)-*block*-poly(2-hydroxyethyl methacrylate) film with PMMA and poly(2-hydroxyethyl methacrylate) domains was soaked into a pyridine/*m*-xylene/perhydropolysilazane mixture and calcinated at 90°C under steam.

One of the important difficulties faced in earlier work in preparing polymer nanocomposites is that particles are hydrophilic (because of the —OH group on the surface) in nature and tend to agglomerate instead of dispersing homogeneously within it. To overcome this problem, the surface of these particles must be suitably modified. There are two ways to do this, and the first one is surface absorption or a reaction with small molecules, such as a silane coupling agent. In this method, the molecules have two parts: one that combines with the surface chemically and another that is compatible with the polymer.[46] The second method is based on grafting polymeric molecules through covalent bonding to the hydroxyl groups existing on the particles. This grafting can be conducted either by the polymerization of the monomer before its attachment to the nanoparticles or by the use of a readymade polymer with suitable functional groups reacting to the hydroxyl group of the nanoparticles. The various kinds of polymerization processes, including radical, anionic, and cationic processes, through which grafted polymers are propagated from the surfaces of particles were reported by Tsubokawa and coworkers.[47,48] An effective surface modification method grafting polystyrene and polyacrylamide onto nanoalumina particles was developed by Rong et al.[49]

In this work, we produced alumina nanoparticles through the autoignition of aluminum nitrate and urea in a furnace. We found that these were highly hydrophilic, having hydroxyl groups on the surface, and caused considerable agglomeration in the PMMA matrix. To bond alumina with the polymer matrix covalently, the surface was modified with methacrylol isocyanate, which was synthesized by the reaction of methacrylol chloride and sodium azide, which reacted with nanoalumina particles readily. The nanoparticles after the modification reaction had double bonds on the surface, which polymerized to produce a covalent link with the matrix produced. We tested a composite having two layers with a bullet-firing machine and a vertical-drop-weight-impact testing machine, and it showed considerably superior properties. Encouraged by this result, we prepared a 10-layer composite that was not damaged by 0.32 Indian Ordinance Factory (IOF) revolvers from a 10-m distance with a bullet mass of 9.9 g and a muzzle velocity of 236 ± 7 m/s (muzzle energy = 275 J). The value of the critical impact energy to break the multilayered composite was per-

formed with the equation $E = pn^2 + qn + r$, where E is the impact energy, p, q, and r are constants, and n is the number of layers in the composite. Our experiment has shown that these constants are measures of the bonding at the interface, which appears to increase for nanoparticles.

EXPERIMENTAL

Materials

Commercially available aluminum nitrate and urea were used in the preparation of the nanoalumina particles. The MMA monomer was supplied by Fluka Chemicals (Steinheim, Germany). Benzoyl peroxide (BPO) and azobisisobutyronitrile (AIBN) were recrystallized from methanol. Ethylene glycol dimethacrylate (EGDM), supplied by Sigma–Aldrich Chemie (Steinheim, Germany), was used for crosslinking, and dimethyl aniline (DMA) was used as one of the components of the initiator. PMMA sheets were supplied by a local company (Dia Glass Co. India, Ltd., Kanpur, India).

Preparation of the alumina particles

Alumina nanoparticles were prepared through the autoignition reaction of aluminum nitrate and urea. To take advantage of the exothermic reaction, the proper composition of the oxidizer/fuel mixture was important. In this case, aluminum nitrate was used as the oxidizer, and urea was chosen as the fuel. The total oxidizing and reducing valencies of the reactants were adjusted according to the procedure developed by Jain et al.[50] To ensure that the energy released by the reaction was the maximum, they used a quantity termed the equivalent ratio and defined it as the ratio of the total oxidizing valency to the total reducing valency, which in our case was equal to 3. In a typical experiment, the constituents were mixed with water in a pastelike consistency in a beaker and placed in a furnace maintained at 500°C. The paste melted and eventually underwent decomposition, with the evolution of gases resulting in a foamed structure, which then ignited. The entire combustion was over within a few minutes. The processed foams were crushed into powders and were ready for use in the experiments.

Modification of the alumina particles

The nanoalumina particles obtained from the autoignition process were modified with methacrylol isocyanate. For the synthesis of methacrylol isocyanate, first the methacrylol chloride was prepared through the reaction of methacrylic acid (48.5 g, 0.5 gmol) with an equal number of moles of thionyl chloride (98 g, 0.5 gmol) at 0°C for 2 h.[51] After that, sodium azide (35 g) and dry benzene (20 mL) were placed in a conical flask, and to this, an equal number of moles of methacrylol chloride (92 g) was added dropwise from a dropping funnel. The reaction was carried out at 0°C for 8 h; then, it was filtered, and the permeate was methacrylol isocyanate.[52] The mixture of nanoalumina particles and methacrylol isocyanate was stirred at 0°C for 6–8 h, and the final product was dried in an oven at 60°C. The material thus obtained was crushed into powders to obtain modified nanoalumina.

Characterization of the alumina particles

X-ray diffraction (XRD) of alumina

XRD was used to identify the solid crystalline phases in a sample. We used a Reich Seifert (Ahrensburg, Germany) Iso Debye Flex X-ray diffractometer machine, which was operated at 30 kV and 20 mA with Ni-filtered monochromatic Cu Kα radiation at a wavelength of 1.5418 Å with a scan rate of 3°/min in 2θ, and the count per minute was 50 K. Figure 1(b,c) shows the XRD patterns for nanoalumina and modified nanoalumina particles.

BET of alumina

The surface area was measured by the single-point BET method through the physisorption of nitrogen gas at 77 K. The measurement was carried out on a Micrometerics Pulse Chemisorb 2705 (Norcross, GA), which worked through a dynamic adsorption technique.

Transmission electron microscopy (TEM) of alumina

The samples for TEM were prepared by the addition of a small amount of the product to 50 mL of methanol, and the particles of alumina were dispersed in methanol by ultrasonication. A copper grid was taken, and a film was deposited on one side of the grid by 2% poly(vinyl formal) (formvar) dissolved in 1,2-dichloroethane. After this, the grid was dried at room temperature for 2–3 h. After the settling of all large particles in the suspension of alumina in methanol previously prepared, a small amount of the solution was introduced by a dropper nearly at the interface of the light and dark regions of methanol on the film-coated side of the grid. The grid was dried for 2–3 h under ambient conditions and was studied with a JEOL JEM2000FX (Tokyo, Japan) transmission instrument operating at a 100-kV voltage. Figure 2 shows a TEM image of the nanoalumina particles.

Fourier transform infrared (FTIR) analysis

The FTIR spectra of the alumina and modified alumina were analyzed. Figure 3(a,b) shows the FTIR

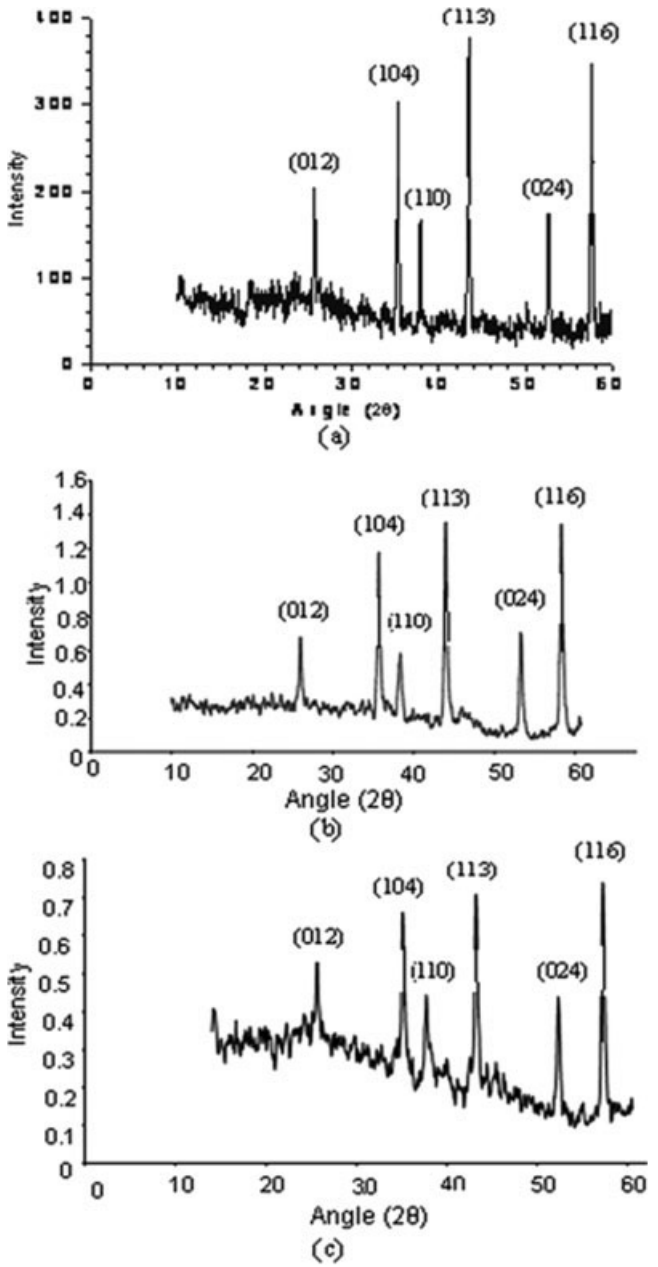

Figure 1 XRD patterns of (a) standard α-alumina, (b) unmodified nanoalumina particles, and (c) chemically modified nanoalumina particles (the peak position is slightly shifted).

spectra of the alumina and modified alumina. From Figure 3(a), it is clear that the —OH group is present at 3433.15 cm^{-1} (lit.[53] 3100–3700 cm^{-1}). Figure 3(b) shows the presence of —NH at 3412.47 cm^{-1} (lit. 3300–3500 cm^{-1}), —CH_2 at 2358.17 cm^{-1} (lit. 2300–3000 cm^{-1}), and C=C at 1630 cm^{-1} (lit. 1450–1650 cm^{-1}).

Thermogravimetric analysis (TGA)

TGA of unmodified and modified nanoalumina particles was carried out at a heating rate of 3°C/min in a temperature range of 40–900°C under a nitrogen atmosphere. Figure 4(a,b) shows the TGA results for the nanoalumina and modified nanoalumina particles, respectively.

Preparation of the polymer nanocomposites

In our work, the monomer (MMA) was polymerized with the following dual-initiating system.[54] MMA (20 g, 0.2 gmol), BPO (0.26 g, 0.1074 gmol), AIBN (0.14 g, 0.085 gmol), and the accelerator DMA (0.082 g, 6.789×10^{-4} gmol) were mixed in a conical flask and then heated gently in a water bath up to around 60°C. Once the viscosity of the polymer changed, nonsettling modified nanoalumina particles (2 wt %, 0.4 g) were added to the polymer solution. Then, the polymerization mixture was well stirred for 1–2 h so that the nanoparticles would be completely mixed. To the final mixture, a crosslinking agent, EGDM (2 g, 0.0101 gmol), was added, and the mixture was then stirred for 5 min more. On heating at 60°C, because of EGDM, the material was crosslinked.

Two thin (2-mm-thick) PMMA sheets (10 cm × 10 cm) were taken, and the final well-mixed polymer syrup was applied between the PMMA sheets in the form of a thin uniform layer; the number of PMMA sheets was increased by the application of the syrup and pressing with a fixed load (4.5 kg). Then, the composite was baked in an oven around 60°C.

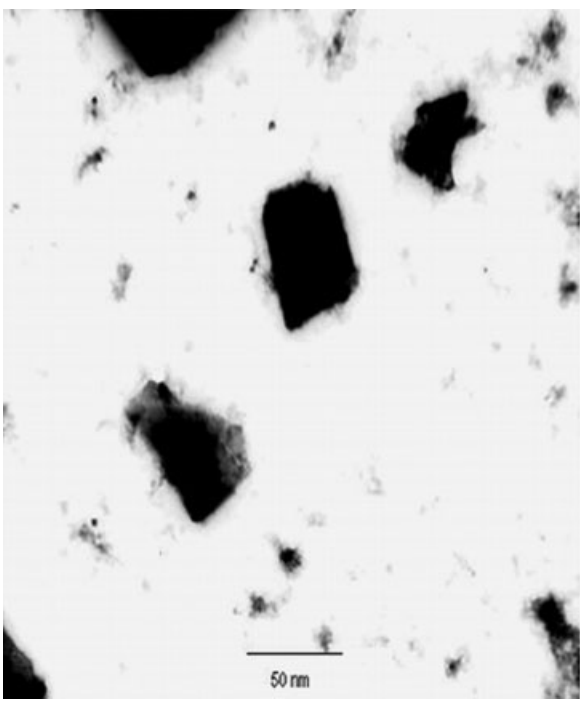

Figure 2 TEM image of unmodified nanoalumina particles. A TEM image of modified nanoalumina looks similar, confirming that little agglomeration is due to chemical modification.

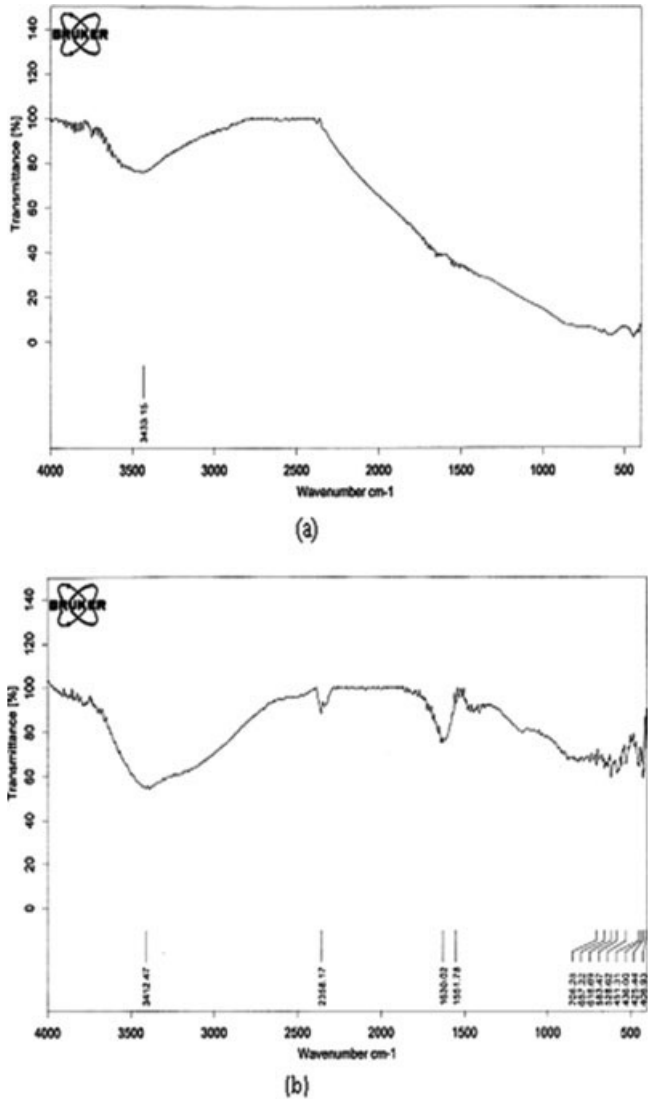

Figure 3 FTIR analysis of (a) nanoalumina particles and (b) modified nanoalumina particles. The modification introduced an isocyanate peak.

Characterization of the polymer nanocomposites

Impact testing of the composite material

The impact testing of the composite materials was carried out with a vertical-drop-weight-impact testing machine. It consisted of a mass weighing 14.5 kg, which dropped onto the specimen from a height calculated with the potential energy equation. Specimens of different layers joined by syrups containing modified nanoalumina particles and not containing nanoalumina were tested with this machine.

Tensile testing of the composite material

A specimen prepared in a dumbbell shape for tensile testing is shown in Figure 5. Samples containing modified nanoalumina particle and not containing nanoalumina were tested by a machine supplied by MTS System Corp. (Eden Prairie, MN) at a rate of 1 mm/min.

RESULTS AND DISCUSSION

Characteristics of the alumina particles

The resulting diffraction patterns (intensity vs 2θ) of alumina powder were recorded on a personal computer with software. The *d* values from the patterns are presented in Tables I and II along with standard *d* values[55] of α-alumina for comparison. It is evident that most of the XRD lines match within 1% of standard α-alumina *d* values. Also, these tables indi-

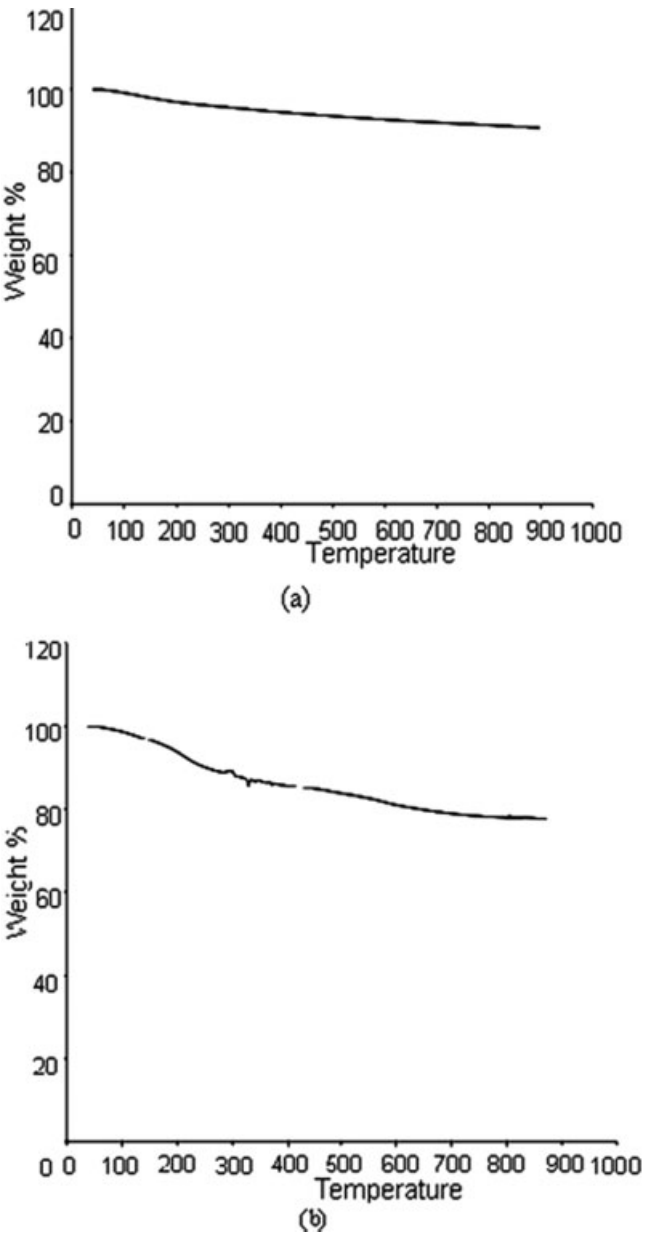

Figure 4 TGA graphs of (a) nanoalumina particles and (b) modified nanoalumina particles. There is slight break in part b at 331°C, showing a loss of the methacrylol isocyanate layer.

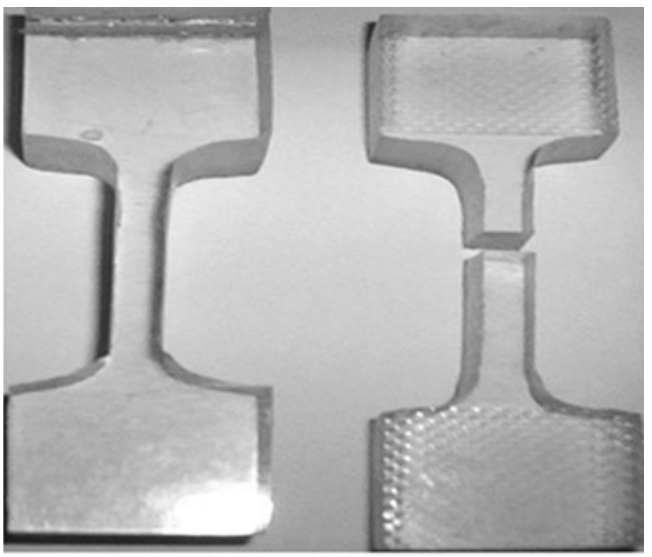

Figure 5 Ten-layer composite specimen (a) before tensile testing and (b) after tensile testing.

cate that the process of surface modification does not affect the crystallographic nature of the alumina powder. The autoignition process used in this investigation is known to produce alumina powder in a quick succession of exothermic reactions. The powder, therefore, is expected to consist of nanoscale particles with possible internal strain due to nonequilibrium cooling. The resultant XRD patterns were, therefore, analyzed to investigate these possibilities with the Scherrer expression.[56] The line broadening of diffraction peaks due to crystalline size effects has been shown to follow this relation:

$$B_{\text{crystalline}} = k\lambda/L\cos\theta \quad (1)$$

where $B_{\text{crystalline}}$ is the broadening of the X-Ray diffraction peaks, λ is the wavelength of the X-rays

TABLE I
Analysis of the XRD Pattern of the Nanoalumina Particles Recorded with Cu Kα Radiation

Peak position (2θ)	*d*		*hkl* plane index
	Theoretical	Experimental	
25.58	3.4793	3.482707	012
35.14	2.5523	2.553750	104
37.75	2.3791	2.382814	110
43.32	2.0850	2.088480	113
52.49	1.7400	1.743243	024
57.42	1.6011	1.604760	116
61.27	1.5100	1.513245	018
66.47	1.4039	1.407321	124

The crystal structure data of the alumina are as follows: the crystal geometry is trigonal, the chemical formula is α-Al_2O_3, and the lattice parameters are $a = b = 4.758$ Å and $c = 12.991$ Å.

TABLE II
Analysis of the XRD Pattern of the Modified Nanoalumina Particles Recorded with Cu Kα Radiation

Peak position (2θ)	*d*		*hkl* plane index
	Theoretical	Experimental	
25.59	3.4793	3.480553	012
35.10	2.5523	2.556586	104
37.72	2.3791	2.385080	110
43.25	2.0850	2.091902	113
52.40	1.7400	1.745979	024
57.38	1.6011	1.605739	116
61.22	1.5100	1.514523	018
66.41	1.4039	1.408134	124

The crystal structure data of the modified alumina are as follows: the crystal geometry is trigonal, the chemical formula is α-Al_2O_3, and the lattice parameters are $a = b = 4.758$ Å and $c = 12.991$ Å.

($\lambda_{\text{Cu K}\alpha} = 1.54$ Å), θ is the Bragg angle, L is the average crystal size, and k is a constant (varying from 0.89 and 1.39) whose value for small cubic crystals of uniform size is 0.94.

The lattice strain in the material also causes broadening of the diffraction peaks, which can be represented by the following relationship:

$$B_{\text{strain}} = \eta\tan\theta \quad (2)$$

where η is the strain in the material, B_{strain} is the broadening of the X-ray diffraction peaks due to the lattice strain in the material. B_r represents the full width at half-maximum and is due to the combined effects of the crystalline size and lattice strain. The

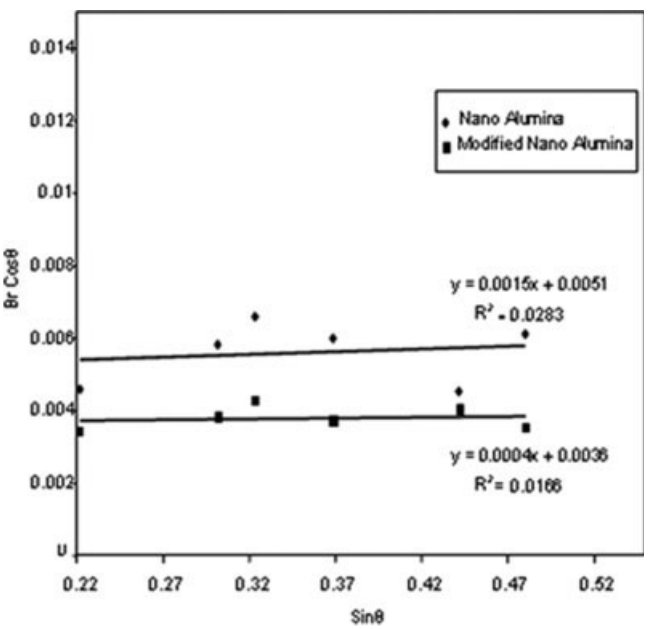

Figure 6 Graph of $B_r \cos\theta$ versus $\sin\theta$ for nanoalumina particles and modified nanoalumina particles.

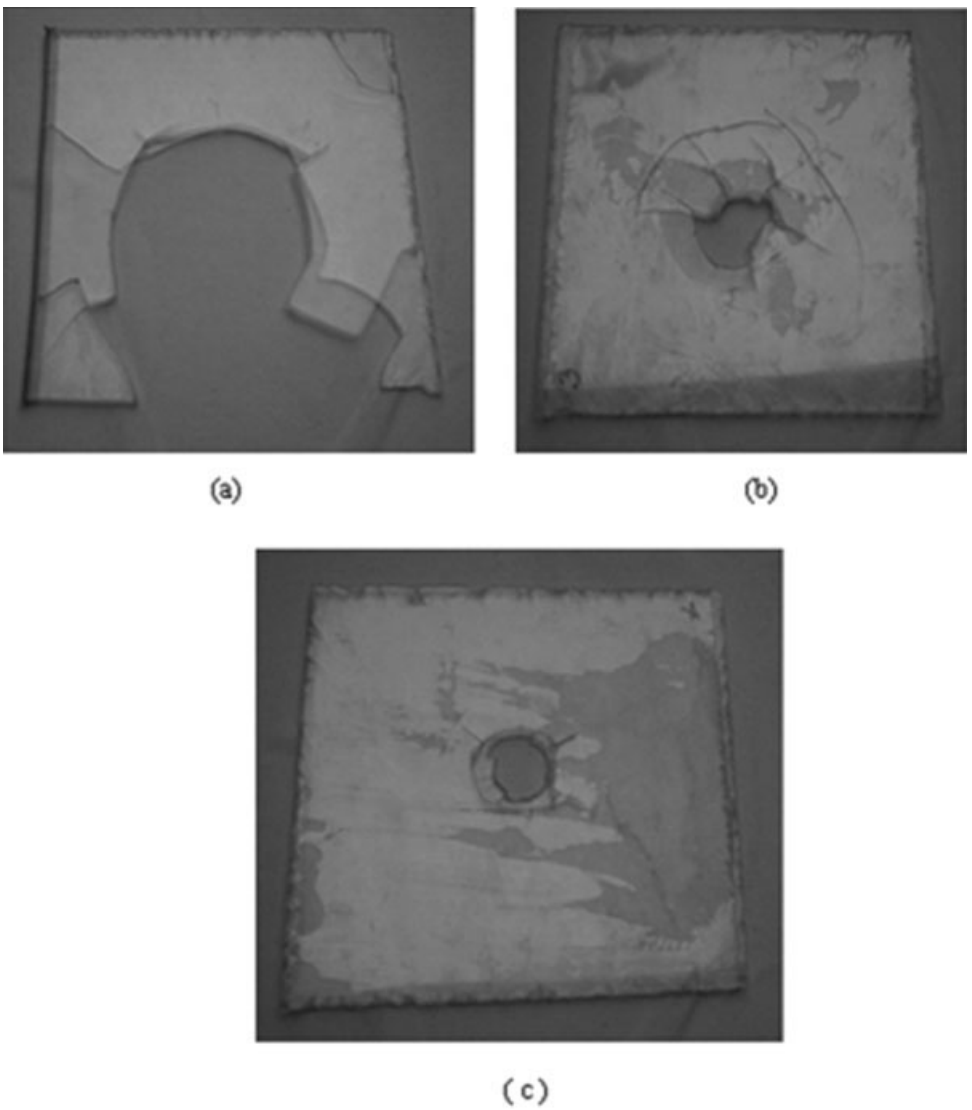

Figure 7 Photographs of two-layer PMMA composites (10 cm × 10 cm × 2 mm for each layer) after being hit by a bullet from a bullet-firing machine: (a) two unjoined sheets put together, (b) sheets joined by polymer syrup without nanoparticles, and (c) sheets joined by polymer syrup containing 2% nonsettling nanoparticles.

expression for B_r is therefore

$$B_r = B_{\text{crystalline}} + B_{\text{strain}} = k\lambda/L\cos\theta + \eta\tan\theta \qquad (3)$$

where $B_{\text{crystalline}}$ and B_{strain} are corrected for instrumental line broadening with an XRD pattern from a polycrystalline silicon wafer with an average particle size of 2.5 μm. From a graph of $B_r \cos\theta$ versus $\sin\theta$, the intercept of the plot yields the value of $(k\lambda)/L$.

The $B_r \cos\theta/\sin\theta$ plots for virgin alumina and surface-modified alumina, shown in Figure 6, are horizontal lines indicating the absence of internal strain. The particle size calculated from the intercepts is 30.5 nm for alumina and 36.4 for modified nanoalumina. From the TEM image, the particle size of nanoalumina has been determined to be 40 nm and is close to the particle size estimated from XRD analysis. The particle size calculated from the BET surface area of alumina (117.23 m^2/g) is 9 nm, which is very small. This indicates the existence of microporous cavities in the alumina grains. The TGA graphs show a 10% weight loss for nanoalumina particles at 900°C and a 23% weight loss for modified nanoalumina particles at 900°C. For modified nanoalumina particles, TGA shows a slight break around 331°C, which indicates the loss of the methacrylol isocyanate layer.

Mechanical properties of the polymer nanocomposite material

Testing of specimens with two layers in the bullet-firing machine

The machine consisted of a gun assembly in which the bullets were propelled to desired velocities with compressed N_2 gas. The speed of the bullet could be fixed within a reasonable range and could be monitored by

photoelectric bulbs. The target was fixed to the frame of the bullet-firing machine. For two layers of PMMA sheets joined by prepared syrups with nanoalumina particles or without nanoalumina, the bullet was fired with 9 J of energy. From the kinetic energy equation

$$E = 1/2mv^2 \quad (4)$$

where m is the mass of the bullet, whose value is 4.73 g, and v is the velocity of the bullet. With this equation, the value of v was found to be 62 m/s for the PMMA sheets. After the bullet was fired with this much velocity, the nonjoined sheets were completely shattered [see Fig. 7(a)]; in contrast, the sheets with the polymer had a 59% damaged area [see Fig. 7(b)], and the sheets with the polymer syrup containing nonsettling nanoparticles had only a 9.6% damaged area [see Fig. 7(c)]. The 10 layers of PMMA sheets joined by the syrup containing nanoalumina were further tested by a 0.32 IOF revolver with a bullet mass of 9.9 g and a velocity of 236 ± 7 m/s (muzzle energy = 275 J). The results showed that the bullet produced an ordinary indentation with no penetration.

Testing of specimens in the vertical-drop-weight-impact testing machine

Here the two-layer PMMA sheets were tested with 3 J of energy (h = 21 mm), where h is the height from which mass of 14.5 kg falls on the composite, and the variation of the load with the time was recorded. Figure 8(a,b) shows the variation of the force with the time for the PMMA sheets with the polymer and the PMMA sheets with the polymer syrup containing 2% nonsettling nanoparticles. From these graphs, the maximum load for the PMMA sheets with the polymer was found to be 90.82 kg, and the maximum load for the PMMA sheets with the polymer syrup containing nonsettling nanoparticles was found to be 166.99 kg. This result gave us the impetus to work further in this direction, and we increased the number of layers by joining the sheets with syrups containing nanoalumina or not containing nanoalumina. Ten samples of each composite specimen consisting of different layers of PMMA sheets joined by a polymer slurry or by a 2% alumina dispersed polymer slurry were tested in the vertical-drop-weight-impact testing machine, and the critical value of the impact resistance energy for a fixed thickness was determined with error bars of approximately 5%. The result is shown in Figure 9, which gives the variation of the impact resistance energy with the number of layers in each pack of specimens in which constituent sheets were joined with the pure polymer adhesive slurry or with the 2% alumina dispersed polymer adhesive slurry. There are two distinct behaviors: the resistance impact increases continuously with an

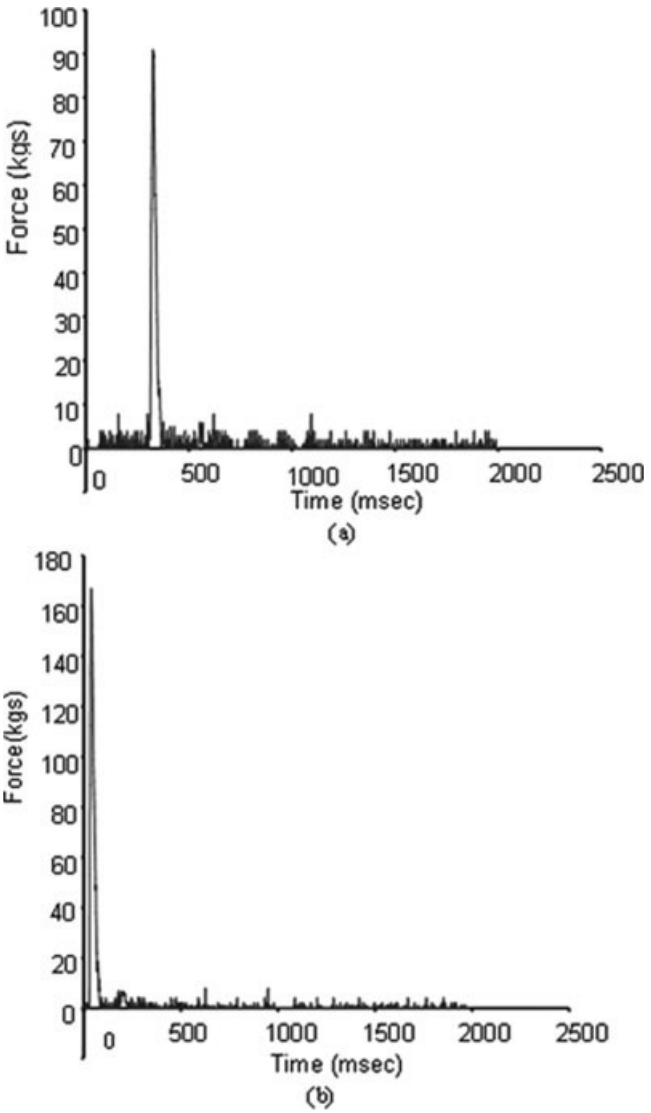

Figure 8 Graph of the force versus the time during drop weight impact testing for two-layer composites (a) joined by polymer syrup without nanoparticles and (b) joined by polymer syrup containing 2% nonsettling nanoparticles.

increasing slope as the number of layers in each composite pack increases, and the increasing rate of the impact energy for the composite packs formed by the 2% alumina dispersive polymer is more pronounced than that for the composite packs joined with the bare polymer adhesive. The composite pack of 10 layered sheets joined by the alumina-dispersed polymer adhesive, as shown in Figure 10(a), survives an impact of 90 J without noticeable damage. This is likely to be a much sought armor material against civilian and possibly 9-mm prohibited-category weapons. In contrast, a similar 10-layer composite pack joined by the mere polymeric adhesive fails through glasslike brittle fracture, as shown in Figure 10(b), at a much lower impact of 50 J. The strengthening mechanism of the composite sheets packed together and joined at the planar interface by the polymeric adhesive or particu-

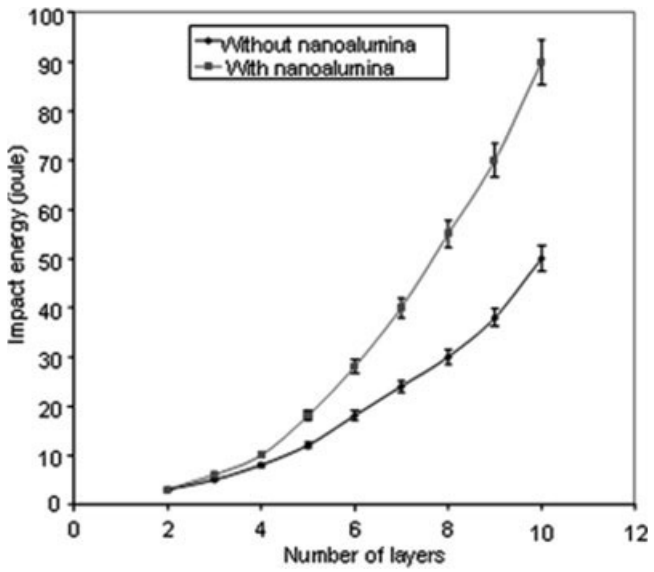

Figure 9 Variation of the impact energy with the number of layers of PMMA sheets in the composites.

late dispersed polymeric adhesive seems to disrupt stress propagation at the constrained (joined) interface. When the interface is free, the explosive impact propagates in the media, breaking open cracks on the free surface. The resistance to impact is, therefore, quite small. When several sheets are packed together, joined by the polymeric or particulate-dispersed polymeric adhesive, the interfaces are no longer free. The large impact strength of the composite reported in this work occurs purely because the syrup and polymer sheet have similar chemical structures forming homogeneous bonding at the interface. Now at each interface, (1) stress propagation changes from a purely forward mode to a partially transverse mode, and (2) the strength of the forward stress and along the sheet interface greatly decreases because of dispersoids in the adhesive. Thus, after each layer, the bonded interface offers increasing resistance to impact. Also, the alumina nanoparticles are chemically bonded to methacrylol isocyanate, producing a carbamate linkage. The modified nanoparticles now have double bonds and are expected to polymerize, forming a linkage between the nanoparticles and matrix. In this way, the interaction energy between the matrix and alumina particles is on the order of the binding energy of the carbamate linkage. As result of this high level of interaction, the impact strength of this composite is considerably enhanced.

The dispersion strengthening in polymer media is a case that fits between a metal and a fluid. In a metal, it has been attributed to the flow of structural dislocations past dispersoids in terms of the Orwan–Ashby model and has been extended to alloys by Gladman.[57] Polymers differ from metals because of their long chain lengths. In the case of a polymer, the flow process can be imagined as long chains slipping over because of the failure of bonding from side groups. Inclusions of dispersoids provide added resistance to this process because long polymer chains in our case are covalently bonded by carbamate linkages to these stronger ceramic particles, reducing stress-driven flow. This situation was illustrated by Lefebvre[58] and Ash et al.[12] in their work involving dispersoids in polymers.

After the analysis of Figure 11(a,b), a model can be proposed for the critical impact energy to fracture as a function of the number of layers in the composite. A power series model takes the following form:

$$E = kn^m$$

where k and m are constants of 2.31 and 1.309, respectively, for polymeric sheets and polymeric ad-

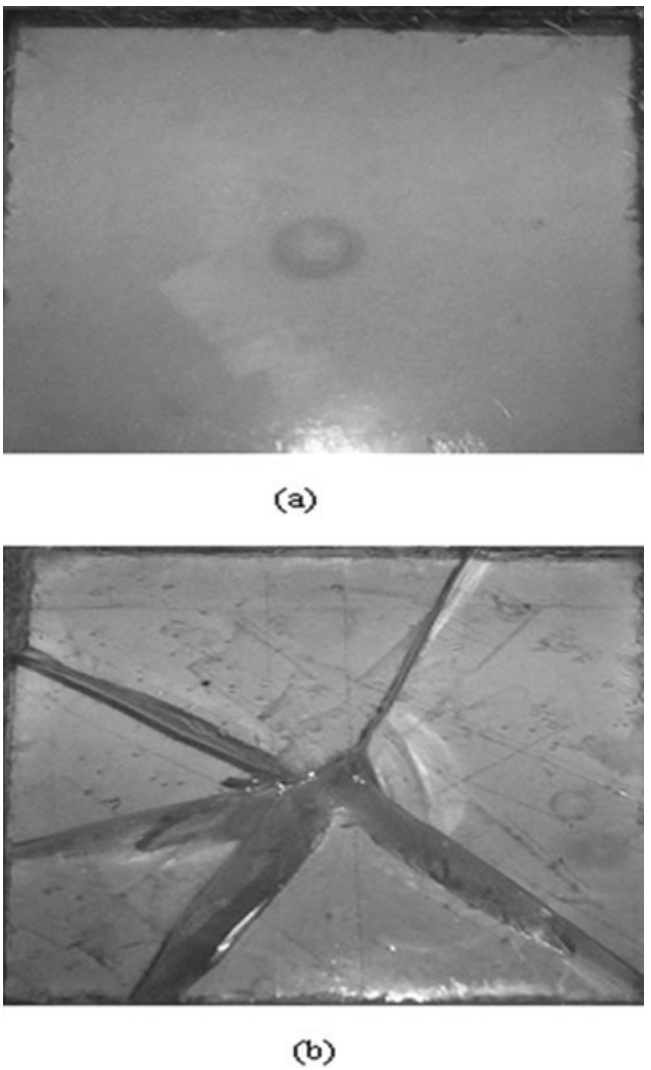

Figure 10 Composite of 10 layers of PMMA sheets (a) joined by polymer syrup containing modified nanoalumina and hit with 90 J of energy, showing no fracture, and (b) joined by polymer syrup without nanoalumina particles and hit with 50 J of energy, showing glasslike fracture.

hesive ($R^2 = 0.9723$) and 2.254 and 1.605, respectively, for polymeric sheets and 2% alumina dispersed polymeric adhesive ($R^2 = 0.9779$). This model is generally good enough for lower energy but shows deviations in a higher energy range. Similarly, an exponential model also shows deviations for higher energy values. The most suitable model that is valid in the whole region of the critical energy value is in the form of a polynomial:

$$E = pn^2 + qn + r$$

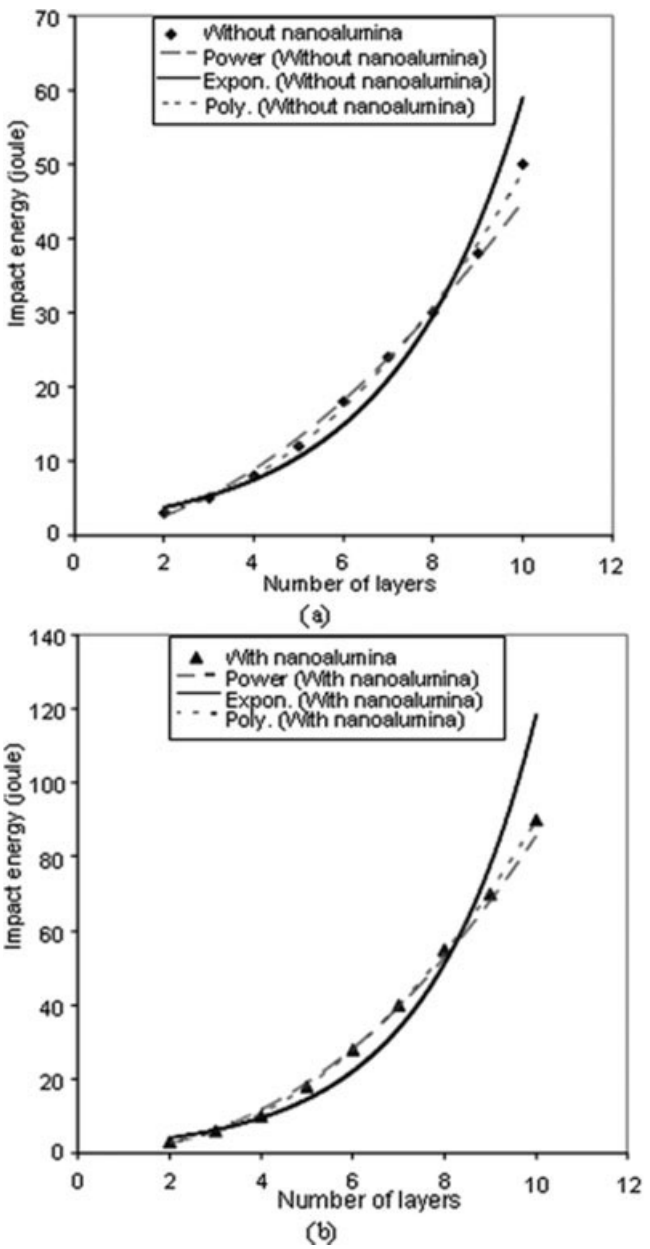

Figure 11 Trend lines for the curve of the impact energy versus the number of layers for composites (a) without nanoalumina and (b) with nanoalumina. For both curves, the polynomial is best fit.

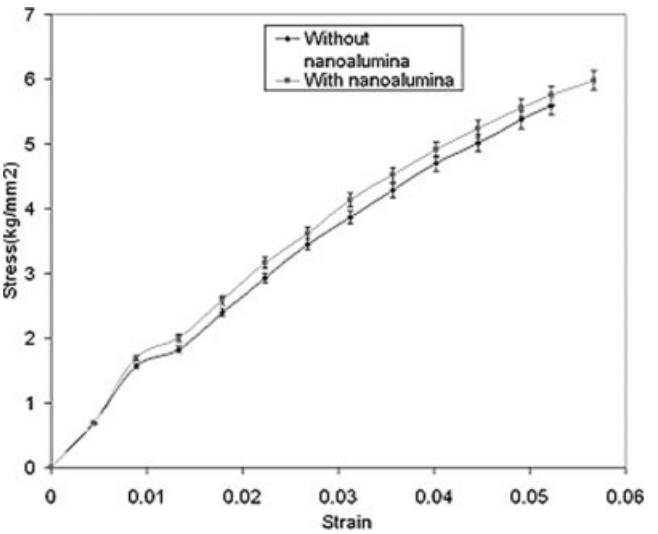

Figure 12 Typical tensile stress–strain curves of composites with nanoalumina and without nanoalumina, showing about 10% higher stress for the nanoalumina-dispersed adhesive at all strain points.

where p, q, and r are 0.551, 0.208, and 2.405, respectively, for polymeric sheets and polymeric adhesive ($R^2 = 0.9978$) and 1.158, −0.713, and 2.452, respectively, for polymeric sheets and 2% alumina dispersed polymeric adhesive ($R^2 = 0.9997$). The values of these constants depend on the materials constituting the sheet elements and the types of adhesives and dispersoids used.

Tensile testing of the specimens

In Figure 12, the tensile stress–strain curve for composites using polymeric and nanoalumina-dispersed adhesives was developed after the testing of five samples for both cases, and the error bar is 2.5%. It is also evident from the figure that the composite block using the nanoalumina-dispersed adhesive shows higher stress values (ca. 10%) at all strain points. This indicates that the alumina-dispersed adhesive offers 10% better resistance against tensile deformation than the pure polymeric adhesive. Although the polymer-adhesive-bonded composite fractures at 5.2% strain, the composite bonded by the alumina-dispersed adhesive breaks at about 5.7% strain and is proved to be a better material. From the linear portion of the curve, where Hook's law is valid, the value of Young's modulus is 1.54 GPa, and in this region, the whole load is taken by the bulk material itself.

CONCLUSIONS

In this study, alumina nanoparticles with a grain size of 30.5 nm were successfully prepared by the autoignition of aluminum nitrate and urea. These

particles were modified with methacrylol isocyanate, which was synthesized by the reaction of methacrylol chloride and sodium azide. The XRD analysis showed that the modified nanoparticles had a similar crystal structure with an average grain size of 36 nm. The TEM analysis showed that the particle size of nanoalumina was in the range of 40 nm, and this confirmed the estimation based on XRD. TGA of nanoalumina showed that there was only 10% weight loss for nanoalumina up to 900°C, whereas there was 23% weight loss for the modified nanoalumina up to 900°C. A polymer syrup containing nonsettling nanoparticles was prepared with 2% modified nanoalumina and MMA polymerized by a dual-initiating system containing BPO, AIBN, and the accelerator DMA. This polymer syrup was applied between PMMA sheets. These composite sheets were tested with a bullet-firing machine and a vertical-drop-weight-impact testing machine. The results of the bullet-firing machine when the bullet was fired at a speed of 62 m/s indicated that empty PMMA sheets were completely damaged, PMMA sheets with the polymer syrup showed 59% damage, and the PMMA sheets with the polymer syrup containing nonsettling nanoparticles had only a 9% damaged area.

The results of the drop-weight-impact testing machine showed that two PMMA sheets with the polymer had a maximum load of 90 kg and that PMMA sheets with the polymer syrup containing nonsettling nanoparticles had a maximum load of 166 kg. With the number of sheets further increased through joining with the polymer syrup containing 2% nonsettling alumina particle, the 10-layer composite showed that it was not affected by an impact energy of 90 J. The experiments were carried out through the determination of the critical impact energy that introduced incipient failure to the composites with an increasing number of layers. It was argued that the impact strength depended on the number of interfaces and the nature of the bonding and could be correlated as follows:

$$E = pn^2 + qn + r$$

The experiment showed that in the presence of the nanoparticles, the value of the constant (a measure of the nature of the interfaces) increased.

The composite material having 10 layers of PMMA sheets joined by the polymer syrup containing nanoalumina was further tested with a 0.32 IOF revolver with a bullet mass of 9.9 g and a velocity of 236 ± 7 m/s. The test confirmed that the bullet of the 0.32 IOF revolver failed to penetrate the sample, and the composite is likely to be used as a bullet-proof material against civilian-grade weapons.

References

1. Akita, H.; Hattori, T. J Polym Sci Part B: Polym Phys 1999, 37, 189.
2. Akita, H.; Kobayashi, H.; Hattori, T.; Kagawa, K. J Polym Sci Part B: Polym Phys 1999, 37, 199.
3. Akita, H.; Kobayashi, H. J Polym Sci Part B: Polym Phys 1999, 37, 209.
4. Pukanszky, B. In Polypropylene: An A–Z Reference; Karger-kocsis, J., Ed.; Kluwer Academic: Dordrecht, 1999; p 574.
5. Savadori, A.; Scapin, M.; Walter, R. Macromol Symp 1996, 108, 1.
6. Vollenberg, P. H. T.; Dehaan, J. W.; Vandeven, L. J. M.; Heikens, D. Polymer 1989, 30, 1663.
7. Kim, G. M.; Lee, D. H.; Hoffmann, B.; Kressler, J.; Stoppelmann, G. Polymer 2000, 42, 1095.
8. Chang, J. H.; An, Y. U. J Polym Phys 2002, 40, 670.
9. Zavyalov, S. A.; Pivkina, A. N.; Schoonman, J. Solid State Ionics 2002, 147, 415.
10. Niihara, K. J Ceram Soc 1991, 99, 974.
11. Sumita, M.; Shizuma, T.; Miyasaka, K.; Ishikawa, K. J Macromol Sci Phys 1983, 22, 601.
12. Siegel, R. W.; Chang, S. K.; Ash, B. J.; Stone, J.; Ajayan, P. M.; Doremus, R. W.; Schadler, L. S. Scr Mater 2001, 44, 2061.
13. Cushing, B. L.; Koleshnichenko, V. L.; O'Connor, C. J. Chem Rev 2004, 104, 3893.
14. Ring, T. A. Fundamentals of Ceramic Powder Processing and Synthesis; Academic: San Diego, 1996.
15. Dirksen, J. A.; Ring, T. A. Chem Eng Sci 1991, 46, 2389.
16. Karpinski, P. H.; Wey, J. S. In Handbook of Industrial Crystallization, 2nd ed.; Myerson, A. S., Ed.; Butterworth-Heinemann: Stoneham, MA, 2001.
17. Tromp, R. M.; Hannon, J. B. Surf Rev Lett 2002, 9, 1565.
18. Blackadder, D. A. Chem Eng 1964, CE303.
19. Brinker, C. J.; Scherer, G. W. Sol–Gel Science: The Physics and Chemistry of Sol–Gel Processing; Academic: San Diego, 1990.
20. Wright, J. D.; Sommerdijk, N. A. J. M. Sol–Gel Materials: Chemistry and Applications; Taylor-Francis: London, 2001.
21. Pierre, A. C. Introduction to Sol–Gel Processing; Kluwer: Boston, 1998.
22. Yan, C.; Sun, L.; Cheng, F. Handbook of Nanophase and Nanostructured Materials; New Delhi: India, 2003; p 72.
23. Liu, X. M.; Wu, S. L.; Chu, P. K.; Zheng, J.; Li, S. L. Mater Sci Eng 2006, 426, 274.
24. Wang, J.; Sha, J.; Yang, Q.; Wang, Y.; Yang, D. Mater Res Bull 2005, 40, 1551.
25. Rajamathi, M.; Seshadri, R. Solid State Mater Sci 2002, 2, 337.
26. Cansell, F.; Chevalier, B.; Demourgues, A.; Etourneau, J.; Even, C.; Garrabos, Y.; Pessey, V.; Petit, S.; Tressaud, A.; Weill, F. J. Mater Chem 1999, 9, 67.
27. Cheng, H.; Ma, J.; Zhao, Z.; Qi, L. Chem Mater 1995, 7, 663.
28. Yang, J.; Cheng, G.-H.; Zeng, J.-H.; Yu, S.-H.; Liu, X.-M.; Qian, Y.-T. Chem Mater 2001, 13, 848.
29. (a) Kumar, P.; Mittal, K. L. Handbook of Microemulsion Science and Technology; Marcel Dekker: New York, 1999; Part III, p 452;. (b) Texter, J. Reactions and Synthesis in Surfactant Systems; Surfactant Science Series 100; Marcel Dekker: New York, 2001; Part IV, p 577.
30. Langevin, D. In Structure and Reactivity in Reverse Micelles; Pileni, M. P., Ed.; Elsevier: Amsterdam, 1989.
31. North, A. M. The Collision Theory of Chemical Reactions in Liquids; Methuen: London, 1964.
32. Winsor, P. A. Chem Rev 1968, 68, 1.
33. Towey, T. F.; Khan-Lodhi, A. N.; Robinson, B. H. J Chem Soc Faraday Trans 1990, 86, 3757.
34. Agostiano, A.; Catalano, M.; Curri, M. L.; Della Monica, M.; Manna, L.; Vaasanelli, L. Micron 2000, 31, 253.
35. Vollenberg, P. H. T.; Heikens, D. Polymer 1989, 30, 1656.

36. Chan, C.-M.; Wu, J.; Li, J.-X.; Cheung, Y.-K. Polymer 2002, 43, 2981.
37. Petrovic, Z. S.; Javni, I.; Waddon, A.; Banhegyi, G. J Appl Polym Sci 2000, 76, 13.
38. Yang, F.; Ou, Y.; Yu, Z. J Appl Polym Sci 1998, 69, 355.
39. Ou, T.; Yang, F.; Yu, Z. J Polym Sci Part B: Polym Phys 1998, 36, 789.
40. Reynaud, E.; Jouen, T.; Gautheir, C.; Vigier, G. Polymer 2001, 42, 8759.
41. Li, J.-X.; Wu, J.; Chan, C. M. Polymer 2000, 41, 6935.
42. Okada, A.; Usuki, T.; Kurauchi, O.; Kamigaito. In ACS Symposium, Hybrid Organic-Inorganic Composites. Mark, J. E.; Lee, C. Y.-C.; Branconi, P. A., Eds.; Washington, D.C., 1995; p 55.
43. Vu, Y. T.; Mark, J. E.; Pham, L. H.; Engelhardt, M. J Appl Polym Sci 2001, 82, 1392.
44. Qi, D.-M.; Bao, Y.-Z.; Weng, Z.-X.; Huang, Z.-M. Polymer 2006, 47, 4622.
45. Mori, Y.; Saito, R. Polymer 2004, 45, 95.
46. Kumar, A.; Gupta, R. K. Fundamentals of Polymers, 1st ed.; McGraw-Hill: New York, 1998.
47. Tsubokawa, N.; Shirai, Y.; Hashimoto, K. Colloid Polym Sci 1995, 273, 1049.
48. Tsubokawa, N.; Kogure, A.; Sone, Y. J Polym Sci Part A: Polym Chem 1995, 28, 1923.
49. Rong, M. Z.; Ji, Q. L.; Zhang, M. Q.; Friedrich, K. Eur Polym J 2002, 38, 1573.
50. Jain, S. R.; Adiga, K. C.; Verneker, V. R. P. Combust Flame 1981, 40, 71.
51. Finar, I. L. Organic Chemistry, 6th ed.; ELDS: New Delhi, India, 1989; Vol. 1, p 256.
52. Finar, I. L. Organic Chemistry, 6th ed.; ELDS: New Delhi, India, 1989; Vol. 1, p 165.
53. http://wwwchem.csustan.edu/tutorials/infrared.htm (July 15, 2005).
54. Pugazhenthi, G.; Kumar, A. J Membr Sci 2004, 228, 187.
55. Powder Diffraction File; International Centre for Diffraction Data; New Delhi, India, 1985; Vol. 10, p 173.
56. Suryanarayana, C.; Norton, M. G. X-Ray Diffraction: A Practical Approach; Plenum: New York, 1998; p 207.
57. Gladman, T. The Physical Metallurgy of Microalloyed Steels; Institute of Materials: London, 1997; p 47.
58. Lefebvre, J. Encyclopedia of Polymer Science and Technology; Wiley: New York, 2002, Vol. 3, p 336.